BAREKENG: Journal of Mathematics and Its Applications
June 2026 Volume 20 Issue 2 Page 1215–1228
P-ISSN: 1978-7227 E-ISSN: 2615-3017
https://doi.org/10.30598/barekengvol20iss2pp1215-1228

DYNAMIC MODELING OF CARBON DIOXIDE EMISSIONS USING HIGH-ORDER DIFFERENTIAL EQUATIONS AND NONLINEAR ESTIMATION

Udjianna S. Pasaribu[1], **Adilan W. Mahdiyasa**[2*], **Asrul Irfanullah**[3]

[1,2] *Mathematics Study Program, Faculty of Mathematics and Natural Sciences, Institut Teknologi Bandung*
[3]*Master of Actuarial Science, Faculty of Mathematics and Natural Science, Institut Teknologi Bandung*
Jln. Ganesha No 10, Bandung, 40132, Indonesia

*Corresponding author's e-mail: * **adilan.widyawan@itb.ac.id***

Article Info

Article History:

Received: 6th May 2025
Revised: 28th July 2025
Accepted: 27th September 2025
Available online: 26th January 2026

Keywords:

Carbon dioxide;
Differential equation;
Emission dynamics;
Nonlinear estimation;
United States.

ABSTRACT

Carbon dioxide (CO_2) is one of the main factors contributing to global warming. As the second largest CO_2 emitter globally, the United States (US) faces increasing political and economic pressure to reduce its emissions. Historical emission data exhibits complex structural patterns characterized by linear growth, quadratic trends, and periodic oscillations. Most existing models fail to capture this multifaceted behavior. In this study, we propose a high-order differential equation to represent the dynamic behavior of CO_2 emissions in the US. The model integrates linear, quadratic, and oscillatory components to reflect both long-term and short-term fluctuations. Nonlinear parameter estimation techniques are employed to fit the model to historical emission data with high accuracy. The proposed model effectively captures historical emission behavior, demonstrating strong goodness of fit and identifying both trend and cyclical components. Model-based projections indicate a likely resurgence in emission growth over the next decade, raising concerns regarding compliance with climate commitments and potential exposure to international carbon pricing instruments. The findings highlight the value of combining differential equation modeling with nonlinear estimation in analyzing environmental systems. The main limitation of this study is that it focuses only on historical emission dynamics, without direct integration of socio-economic drivers. This gap, however, highlights opportunities for future research.

How to cite this article:

U. S. Pasaribu, A. W. Mahdiyasa, and A. Irfanullah, "DYNAMIC MODELING OF CARBON DIOXIDE EMISSIONS USING HIGH-ORDER DIFFERENTIAL EQUATIONS AND NONLINEAR ESTIMATION", *BAREKENG: J. Math. & App.*, vol. 20, no. 2, pp. 1215-1228, Jun, 2026.

Journal homepage: *https://ojs3.unpatti.ac.id/index.php/barekeng/*
Journal e-mail: *barekeng.math@yahoo.com; barekeng.journal@mail.unpatti.ac.id*

Research Article · **Open Access**

1. INTRODUCTION

Global warming is one of the biggest issues facing the world today, characterized by a sustained increase in the Earth's average surface temperature since the pre-industrial era. According to the Intergovernmental Panel on Climate Change (IPCC), the global average temperature has increased by approximately 1.1°C compared to pre-industrial levels, with more than half of this rise occurring in the last four decades. The World Meteorological Organization (WMO) reported that 2024 was the hottest year ever recorded, with global temperatures averaging 1.2°C above pre-industrial baselines [1]. The consequences of such climatic changes extend beyond damaged ecosystems and daily human activities to include rising sea levels, altered precipitation patterns, environmental degradation, and a marked increase in the frequency and severity of natural disasters [2]–[11].

Carbon dioxide (CO_2) is the main greenhouse gas contributing to global warming, driven mostly by fossil fuel combustion, energy consumption, and land-use change. Since the pre-industrial era, atmospheric CO_2 concentration has increased from approximately 277 ppm to around 472 ppm in 2021 [12]. Global CO_2 emissions have climbed from 6 billion tons in 1950 to over 35 billion tons by 2023. This alarming growth has placed immense political and environmental pressure on the world's largest emitters to implement emission-reduction strategies [13]. The United States (US), as the second largest CO_2 emitter globally, contributing roughly 13% of global emissions, plays a pivotal role in shaping international climate outcomes.

The US has experienced increasingly severe impacts from climate-related events. In 2023 alone, economic losses from hydrometeorological disasters were estimated at $114 billion, including $73 billion from severe storms, $14 billion from extreme drought, and $5.5 billion in losses due to the Lahaina wildfire in Hawaii [14]. By November 2024, the US had confirmed 24 separate billion-dollar weather and climate disasters, ranging from severe storms to tropical cyclones and wildfires [15]. As CO_2 continues to intensify the global climate system, understanding its temporal dynamics becomes not only scientifically important but also strategically essential for guiding policy and mitigation.

Numerous studies have been carried out to model CO_2 emissions, but the literature remains dominated by regression-based statistical approaches, including Decoupling, the Environmental Kuznets Curve (EKC), and the STIRPAT model [16]–[20], For example, Wei *et al.* [16] valuated the long-run effects of GDP and different energy types on Italy's CO_2 emissions, while Wang *et al.* [17] integrated the Tapio decoupling method with an extended STIRPAT model to analyze economic growth and CO_2 emissions under various scenarios. Similarly, Rao *et al.* [21] used a ridge-regressed STIRPAT model with scenario analysis to forecast Hubei's emissions peaking by 2025. Although these models have successfully identified the drivers of CO_2 emissions, they frequently fail to capture the temporal evolution and periodic oscillations found in long-term emissions data.

Capturing the complex, time-dependent behavior of CO_2 emissions requires analytical tools capable of accurately modeling such dynamics. Differential equations (DEs) provide a powerful mathematical framework for this purpose by explicitly describing the rates of change in a system. For instance, Goreau [22] laid the foundation for dynamic modeling of CO_2 emissions, while Tsokos and Xu [23] applied systems of differential equations to model CO_2 emissions in the United States, using regression-based estimation followed by empirical fitting. Additionally, Han *et al.* [24] proposed a delayed two-dimensional DE to model China's emissions, Donald *et al.* [25] provided a coupled system of nonlinear DEs to model multiple ecological-economic variables, and Mukhartova [26] used a Navier–Stokes-based model to analyze spatial heterogeneity in CO_2 fluxes. While this research contributed dynamic insights into CO_2 emissions, it lacked statistical grounding. The approach in Kafle *et al.* [13] filled this gap by integrating data-driven estimation and functional regression into a fourth-order differential operator to capture varying trends, demonstrating that such models can successfully represent both linear and cyclical emission behaviors.

This study builds upon these earlier efforts by proposing a dynamic modeling framework that integrates high-order differential equations with nonlinear estimation techniques to investigate CO_2 emission patterns in the US. By combining advanced mathematical modeling with empirical environmental data, the research aims to uncover critical emission dynamics such as peaks, accelerations, and turning points, thus enabling a deeper understanding of the nonlinear and evolving nature of CO_2 emissions. Such findings are vital for informing evidence-based climate policy and developing more effective mitigation strategies in the context of an increasingly unstable climate system.

The rest of this paper is organized as follows: Section 2 provides several DE models and their solutions for various cases of data such as linear trends, oscillations, and combinations of both. Section 3 presents the

results and discussion, beginning with the design of a non-homogeneous DE to capture quadratic behavior in the data, followed by parameter estimation, fitting to real data, and prediction. Section 4 summarizes the key findings and implications of the study.

2. RESEARCH METHODS

2.1 DE's Modeling for Various Cases

In analyzing the dynamics of CO_2 emissions, the observed patterns of change can vary widely, ranging from linear growth to more complex fluctuations such as oscillations or a combination of both. Therefore, the DE approach is employed to systematically capture these patterns.

Let $\mathcal{I}(t)$ be the CO_2 emission function, the first-order DE is given by

$$D\mathcal{I}(t) = f(t, \mathcal{I}),$$

with a differential operator D define as the derivative operation with respect to time. We use D to simplify the writing in representing the dynamics of change in $\mathcal{I}(t)$. These operators can be generalized as a linear combination of derivatives of various orders, whose homogeneous form is given by Eq. (1).

$$\beta_0\mathcal{I}(t) + \beta_1 D\mathcal{I}(t) + \beta_2 D^2\mathcal{I}(t) + \cdots + \beta_k D^k\mathcal{I}(t) = 0, \quad (1)$$

where $D^k\mathcal{I}(t)$ is kth-orders derivative of $\mathcal{I}(t)$ and β's are parameters that must be estimated.

a. Linear Trend (Simple Increase or Decrease)

If emissions grow (or decline) at a steady rate without speeding up or slowing down, then the appropriate model satisfies the following equations:

$$D^2\mathcal{I}(t) = 0. \quad (2)$$

Eq. (2) indicates that there is no change in the rate of emission growth, implying a constant rate of change. Solving this gives:

$$\mathcal{I}(t) = C_1 t + C_2, \quad (3)$$

where C_1 is the slope of the trend (if positive, emissions rise, if negative, they fall) and C_2 is the starting level of emission at time $t = 0$.

b. Oscillatory Tren

In many real-world scenarios, CO_2 emissions do not follow a simple linear trend but instead exhibit fluctuations due to economic cycles, technological shifts, or environmental factors. To capture the oscillatory patterns, we use a second-order DE of the form:

$$D^2\mathcal{I}(t) + \beta_2 D\mathcal{I}(t) + \beta_1\mathcal{I}(t) = 0. \quad (5)$$

The solution to these equations depends on the discriminant $\beta_2^2 - 4\beta_1$, which determines whether the system exhibits: 1) Pure Harmonic Oscillations; 2) Damped Oscillations.
If $\beta_1 = -\omega^2$ and $\beta_2 = 0$, Eq. (4) is reduced to:

$$D^2\mathcal{I}(t) = -\omega^2\mathcal{I}(t), \quad (5)$$

where $\omega = \frac{2\pi}{T}$ is the angular frequency that measures the speed of the system's oscillation [27]. Assuming an exponential form of the solution:

$$\mathcal{I}(t) = e^{rt}, \quad (6)$$

where r is a constant to be determined. The exponential form is chosen because it retains its structural properties upon differentiation, which facilitates substitution into the DE. Using Euler's identity gives

$$\mathcal{I}(t) = C_1 \cos(\omega t) + C_2 \sin(\omega t), \quad (7)$$

where $C_1$and C_2 are the oscillation amplitudes, representing the maximum displacement from the equilibrium position. The solution given by Eq. (7) describes a system undergoing harmonic oscillation.

When $\beta_2 \neq 0$, the system exhibits damped oscillations, a phenomenon where emission fluctuations gradually decrease in amplitude over time due to "damping forces" such as emission regulations or technological adaptations. Following the same steps to solve Eq. (5), the characteristic equation is given by

$$r^2 + \beta_2 r + \beta_1 = 0,$$

with roots

$$r_1, r_2 = \frac{-\beta_2 \pm \sqrt{\beta_2^2 - 4\beta_1}}{2}.$$

If the condition $\beta_2^2 - 4\beta_1 < 0$ holds, then the root becomes complex

$$r_1, r_2 = \frac{-\beta_2 \pm i\sqrt{4\beta_1 - \beta_2^2}}{2}.$$

Thus, the solution for the DE with complex roots is a linear combination of two independent solutions

$$\mathcal{I}(t) = e^{r_1 t} + e^{r_2 t}.$$

Substituting the complex roots, the solution can be written as:

$$\mathcal{I}(t) = C_1 e^{\left(\frac{-\beta_2 + i\sqrt{4\beta_1 - \beta_2^2}}{2} t\right)} + C_2 e^{\left(\frac{-\beta_2 - i\sqrt{4\beta_1 - \beta_2^2}}{2} t\right)}.$$

Using Euler's identity, the solution for Eq. (4) is

$$\mathcal{I}(t) = C_1 e^{\phi t} \cos(\xi t) + C_2 e^{\phi t} \sin(\xi t), \tag{8}$$

where $\phi = -\frac{\beta_2}{2}$ and $\xi = \frac{\sqrt{4\beta_1 - \beta_2^2}}{2}$.

c. Combination of Linear and Oscillatory Tren

In parts (a) and (b), we discussed DE models that capture linear trends and oscillatory patterns separately. However, in reality, CO_2 emissions often exhibit more complex behavior in which increasing or decreasing trends are accompanied by oscillations. To model such phenomena, we proposed a higher-order DE, specifically a fourth-order DE:

$$D^4\mathcal{I}(t) + \beta_2 D^3\mathcal{I}(t) + \beta_1 D^2\mathcal{I}(t) = 0. \tag{9}$$

To simplify, we introduce an intermediate variable:

$$D^2\mathcal{I}(t) = u(t).$$

Thus, Eq. (9) is reduced to a second-order DE in terms of $u(t)$:

$$u''(t) + \beta_2 u'(t) + \beta_1 u(t) = 0. \tag{10}$$

Solving the characteristic equations yields a solution structure like Eq. (10)

$$u(t) = C_1 e^{\phi t} \cos(\xi t) + C_2 e^{\phi t} \sin(\xi t).$$

Since $D^2\mathcal{I}(t) = u(t)$, the general solution for $\mathcal{I}(t)$ is obtained by integrating $D^2\mathcal{I}(t)$ twice:

$$\begin{aligned} D\mathcal{I}(t) &= \int \left(C_1 e^{\phi t} \cos(\xi t) + C_2 e^{\phi t} \sin(\xi t)\right) dt \\ &= A e^{\phi t}(B_1 \cos(\xi t) + B_2 \sin(\xi t)) + C_3, \\ \mathcal{I}(t) &= \int \left(A e^{\phi t}(B_1 \cos(\xi t) + B_2 \sin(\xi t)) + C_3\right) dt \\ &= A^2 e^{\phi t}[(B_1\phi - B_2\xi)\cos(\xi t) + (B_1\xi + B_2\phi)\sin(\xi t)] + C_3 t + C_4, \end{aligned} \tag{11}$$

where $A = \frac{1}{\phi^2 + \xi^2}$; $B_1 = C_1\phi - C_2\xi$ and $B_2 = C_1\xi + C_2\phi$.

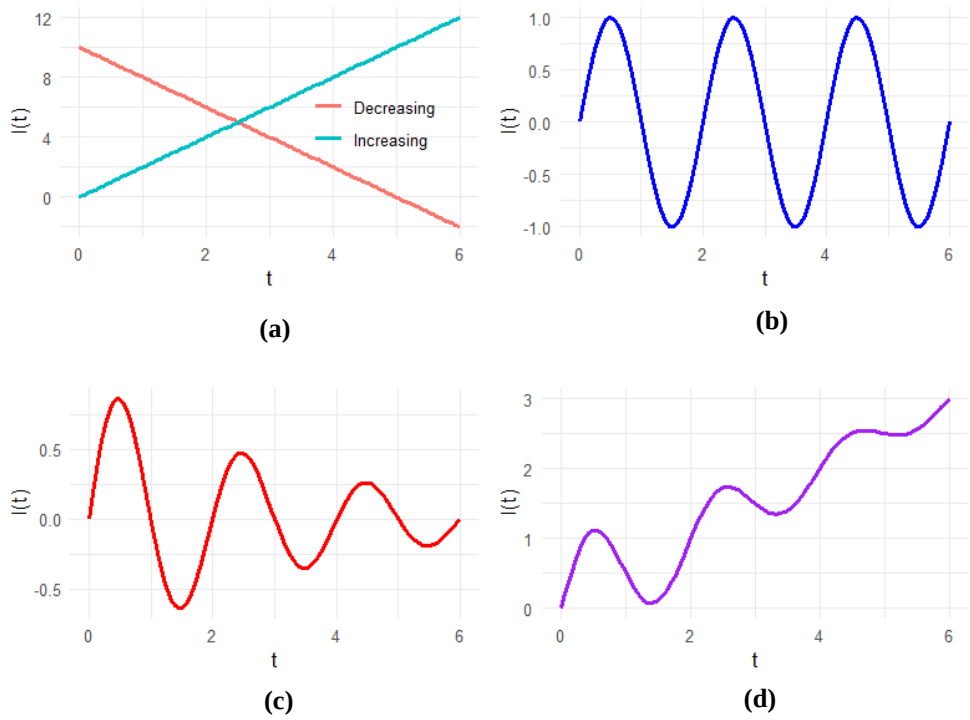

Figure 1. Various Systems of Dynamics Patterns. The Horizontal Axis t Denotes Time, and the Vertical Axis $\mathcal{I}(t)$ Represents Emission Intensity: (a) Linear Trend; (b) Harmonic Oscillation; (c) Damped Oscillation; (d) Combination of Linear Trend and Damped Oscillation

This model offers flexibility in capturing both the linear trend (through the term $C_3 t + C_4$) and damp oscillation ($e^{\phi t}\cos(\xi t)$ and $e^{\phi t}\sin(\xi t)$). As such, it provides a more realistic representation of CO_2 emission dynamics, which are characterized not only by growth but also by fluctuations driven by various External factors.

2.2 Nonlinear Estimation

When we are working under a nonlinear model, parameter estimation often requires iterative techniques to minimize the residual sum of squares between observed and predicted values [28]. The Gauss–Newton method is one of the most widely used algorithms for solving nonlinear least squares problems, particularly when the model can be locally approximated as linear in the neighborhood of the true parameter values [29].

Let $\boldsymbol{\mathcal{I}} = (\mathcal{I}_1, \mathcal{I}_2, \ldots, \mathcal{I}_I)'$ be the vector of observed data, and $\hat{\boldsymbol{\mathcal{I}}}(\boldsymbol{\beta})$ the vector of model prediction based on the parameter vector $\boldsymbol{\beta} \in \mathbb{R}^n$. The aim is to minimize the sum of square errors:

$$\chi^2(\boldsymbol{\beta}) = \sum_{i=1}^{I} \left(\mathcal{I}_i - \hat{\mathcal{I}}(t_i;\boldsymbol{\beta})\right)^2 = \left\|\boldsymbol{\mathcal{I}} - \hat{\boldsymbol{\mathcal{I}}}(\boldsymbol{\beta})\right\|^2. \tag{12}$$

The Gauss-Newton method iteratively updates $\boldsymbol{\beta}$ using:

$$\boldsymbol{\beta}_{k+1} = \boldsymbol{\beta}_k + \boldsymbol{h}_k. \tag{13}$$

Where the update step $\boldsymbol{h}_k$ is obtained by solving the normal equations:

$$(\boldsymbol{J}'\boldsymbol{J})\boldsymbol{h}_k = \boldsymbol{J}'\left(\boldsymbol{\mathcal{I}} - \hat{\boldsymbol{\mathcal{I}}}(\boldsymbol{\beta})\right). \tag{14}$$

Here, $\boldsymbol{J} = \left.\frac{\partial \hat{\boldsymbol{\mathcal{I}}}(\boldsymbol{\beta})}{\partial \boldsymbol{\beta}}\right|_{\beta_k} \in \mathbb{R}^{I\times n}$ is the Jacobian matrix evaluated at iteration k. The Gauss–Newton method typically converges faster than gradient descent when the initial parameter estimates are reasonably close to the true values. However, in the presence of large residuals or strong nonlinearity, convergence may be slow or unstable, necessitating a damped version of the algorithm such as the Levenberg–Marquardt method. In this study, the Gauss–Newton method is applied to estimate parameters in a high-order DE model of CO_2 emissions. The method provides an efficient solution for refining model coefficients, ensuring that the simulated emission trajectory aligns with historical data through least-squares minimization.

2.3 Data

The data used in this paper is sourced from the *Our World in Data* website (accessible at https://ourworldindata.org/co2-emissions), which contains CO_2 emissions data for each country. The country of interest is the US, with an observation period spanning from 1950 to 2023. A summary of the numerical data is presented in Table 1.

Table 1. Data Summary (in 1000 tons)

Statistics	CO_2 Emissions
Min	2,489,462
Max	6,132,183
Mean	4,627,113
Standard deviation	1,100,958
Q_1	3,889,476
Q_2	4,900,672
Q_3	5,413,394
Skewness	0.63
Kurtosis	0.86

Table 1 presents the summary of CO_2 emissions (in 1000 tons), illustrating the distribution and characteristics of the data. It is observed that the average CO_2 emissions over the period from 1950 to 2023 are 4,627,113 thousand tons, with the lowest CO_2 emissions recorded at 2,489,462 thousand tons (in 1954) and the highest at 6,132,183 thousand tons (in 2005). The standard deviation of 1,100,958 thousand tons indicates a significant variation in the data. Q_1, Q_2, and Q_3 are 3,889,476; 4,900,672; and 5,413,394 thousand tons, respectively. Q_2 slightly higher than the mean, suggests that the data distribution is slightly skewed to the right (positive), as confirmed by the skewness value of 0.63. This value indicates that most of the data points lie below the mean, but some relatively large values pull the distribution to the right. The kurtosis value of 0.86 suggests that the data distribution is relatively close to a normal distribution, although it is somewhat more peaked than the standard normal distribution. The distribution of CO_2 emissions is shown in Fig. 2.

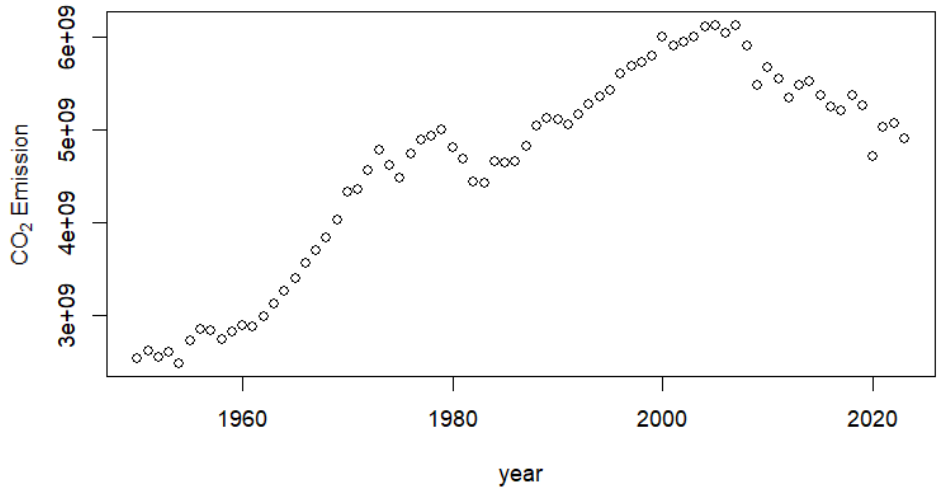

Figure 2. CO_2 emissions in the United States from 1950–2023

The horizontal axis of Fig. 2 shows the year, and the vertical axis shows annual CO_2 emissions (tons). Based on Fig. 2, the data exhibits three main patterns: (1) a linear increasing trend, (2) a quadratic growth curve, and (3) cyclic fluctuations.

3. RESULTS AND DISCUSSION

3.1 Modelling Approach

Subchapter 2.1 has presented several DE models to capture various data patterns, including the linear increasing trend and oscillations as given by Eq. (11)**.** However, as observed in Fig. 2, another pattern emerges, namely the quadratic pattern, indicated by the increase in CO_2 emissions reaching a peak in 2007, followed by a decline towards the end of the observation period. To address this limitation, the solution provided by Eq. (11) is modified by adding a quadratic constant term to Eq. (10), thereby transforming the homogeneous DE into a non-homogeneous one. This modification aims to enhance the flexibility of the model solution, allowing it to better represent the quadratic pattern.

The non-homogeneous DE by adding a constant function can be written as:

$$u''(t) + \beta_2 u'(t) + \beta_1 u(t) = \psi, \tag{15}$$

where ψ is a constant term, the general solution of the non-homogeneous DE consists of two parts: the homogeneous solution and the particular solution. The homogeneous solution $\mathcal{I}_H(t)$ has been derived and is given by Eq. (11). The particular solution $\mathcal{I}_P(t)$ includes the additional contribution from the constant function ψ.

Assume the solution $u_P(t)$ takes the constant form Ψ, that is

$$u_P(t) = \Psi\,. \tag{16}$$

The particular solution is given by

$$\mathcal{I}_P(t) = \frac{\psi}{2\beta_1}t^2 + C_{P1}t + C_{P2}, \tag{17}$$

where C_{P1} , C_{P2} is the integration constant of the solution. The general solution of the non-homogeneous DE is given by:

$$\begin{aligned}
\mathcal{I}(t) &= \mathcal{I}_H(t) + \mathcal{I}_P(t) \\
&= A^2 e^{\phi t}[(B_1\phi - B_2\xi)\cos(\xi t) + (B_1\xi + B_2\phi)\sin(\xi t)] + C_3 t + C_4 + \frac{\psi}{2\beta_1}t^2 + C_{P1}t + C_{P2} \\
&= A^2 e^{\phi t}[(B_1\phi - B_2\xi)\cos(\xi t) + (B_1\xi + B_2\phi)\sin(\xi t)] + \frac{\psi}{2\beta_1}t^2 + (C_{P1} + C_3)t + (C_{P2} + C_4)\mathcal{I}(t) \\
&= \mathcal{I}_H(t) + \mathcal{I}_P(t) \\
&= A^2 e^{\phi t}[(B_1\phi - B_2\xi)\cos(\xi t) + (B_1\xi + B_2\phi)\sin(\xi t)] + C_3 t + C_4 + \frac{\psi}{2\beta_1}t^2 + C_{P1}t + C_{P2} \\
&= A^2 e^{\phi t}[(B_1\phi - B_2\xi)\cos(\xi t) + (B_1\xi + B_2\phi)\sin(\xi t)] + \frac{\psi}{2\beta_1}t^2 + (C_{P1} + C_3)t + (C_{P2} + C_4)
\end{aligned} \tag{18}$$

Note that $A^2(B_1\phi - B_2\xi)$ and $A^2(B_1\xi + B_2\phi)$ are constant, they can be denoted as c_1 and c_2, respectively. Similarly, for $\frac{\psi}{2\beta_1}$, $(C_{P1} + C_3)$ and $(C_{P2} + C_4)$. Thus, Eq. (18) can be written as:

$$\mathcal{I}(t) = c_1 e^{\phi t}\cos(\xi t) + c_2 e^{\phi t}\sin(\xi t) + c_3 t^2 + c_4 t + c_5. \tag{19}$$

The solution given by Eq. (19) represents the general solution of the non-homogeneous DE, capable of capturing patterns of linear growth, quadratic trends, and oscillation. The parameters c_1 and c_2 control the initial amplitude and phase of the oscillations. The expression $e^{-\phi t}$ representing the change in amplitude of the oscillations over time. If $\phi < 0$, this factor reflects exponential damping, meaning the oscillations gradually decrease. If $\phi = 0$, the amplitude remains constant, while if $\phi > 0$, indicating an increase in amplitude, reflecting unstable dynamics.

Additionally, the sinusoidal functions $\cos(\xi t)$ and $\sin(\xi t)$ serve to describe periodic oscillation patterns. These functions represent repetitive fluctuations with a specific frequency, where the value of ξ determines the speed of the oscillation cycles. These sinusoidal functions allow the model to accurately capture short-term cyclic dynamics or periodic fluctuations. The combination of these two functions provides flexibility in adjusting the initial phase and the scale of the oscillations.

The parameter c_3 determines the rate of acceleration or deceleration in the model. If $c_3 > 0$, the function t^2 opens upwards, indicating acceleration; conversely, if $c_3 < 0$, it indicates deceleration. The components c_4 and c_5 represent the linear relationship between time t and the change in the value of $\mathcal{I}(t)$.

3.2 Model Prediction

The solution given by Eq. (19) is subsequently used for estimation and prediction purposes. [13] estimates the parameter $\boldsymbol{\beta}$ and the integration coefficients $\boldsymbol{c}$ separately, where $\boldsymbol{\beta}$ is estimated through functional regression by introducing the differential operator, and $\boldsymbol{c}$ is estimated via nonlinear regression. However, in this paper, all parameters are estimated simultaneously using nonlinear regression to obtain consistent parameter estimates and simplify the estimation process. We use RStudio to estimate the values of the parameters [30]. RStudio was selected as the primary computational environment for this study because it is open-source, user-friendly, and widely adopted in statistical and data science research. Unlike linear regression, there is no explicit form for parameter estimation in nonlinear regression. The computational process requires the careful selection of initial values to avoid slow convergence or failure to find the optimal solution due to being trapped in a local minimum or exhibiting asymptotic behavior. In this case, the initial values are determined through a numerical approach using the Finite Difference Method. This approach enables the calculation of function values and their derivatives at time $t = 0$. Since the order of the DE used is fourth order, the initial values are determined up to the third-order derivatives.

If $\boldsymbol{\beta} = (\beta_1, \beta_2, c_1, c_2, c_3, c_4, c_5)'$ is the vector of parameters to be estimated, then the initial vector is $\boldsymbol{\beta}_{initial}$ given by

$$\boldsymbol{\beta}_{initial} = \left(\left(\frac{2\pi}{49{,}33}\right)^2 ;\ 0.25\ ; D\mathcal{I}(0)\ ; D^2\mathcal{I}(0);\ D^2\mathcal{I}(0);\ D\mathcal{I}(0);\ \mathcal{I}(0) \right)'.$$

The selection of initial values for each parameter is based on the characteristics and roles of each parameter. The parameter β_1 is given by the square of the angular frequency,

$$\beta_1 = \omega^2,$$

where $\omega = \frac{2\pi}{T}$. T is calculated based on the total observation time and the number of oscillations, where the total observation time is 74 years, and the number of oscillations is approximately 1.5:

$$T = \frac{74}{1.5} \approx 49.33\ year.$$

Thus, the initial value for β_1 is given by

$$\beta_1 = \left(\frac{2\pi}{49.33}\right)^2.$$

The initial value of β_2 is selected randomly such that it satisfies the condition: $\beta_2^2 - 4\beta_1 < 0$. The parameter estimation for the DE solution is presented in Table 2. The estimated parameter results from both models, namely the model without the quadratic component (Model I) and the model with the quadratic component (Model II), as presented in Table 2, show significant differences. In Model I, the parameter $\beta_1 = 0.0174$ indicates a lower damping rate of oscillations compared to Model II 0.0240. The smaller value of β_1 in Model I suggests that the amplitude of oscillations in the data decays more slowly over time, which does not align well with the observed data pattern. Meanwhile, β_2 in Model I (-0.2368) is also significantly smaller in magnitude compared to that in Model II (-0.0135). The low β_2 value in Model I indicates that this model attempts to impose a global pattern, such as acceleration and deceleration, into the oscillatory component, leading to distorted parameter estimates.

Table 2. Parameter Estimation

Parameter	Estimation	
	Non-Quadratic (Model I)	Quadratic (Model II)
β_1	0.0174	0.0240
β_2	-0.2368	-0.0135
c_1	-2.992×10^5	1.790×10^8
c_2	7.368×10^5	-2.216×10^8
c_3	-	-9.652×10^5

Parameter	Estimation	
	Non-Quadratic (Model I)	Quadratic (Model II)
c_4	7.098×10^7	1.158×10^8
c_5	2.451×10^9	2.167×10^9
R^2	0.946	0.9770
RMSE	0.2531	0.1659
AIC	-191.3517	-251.9000

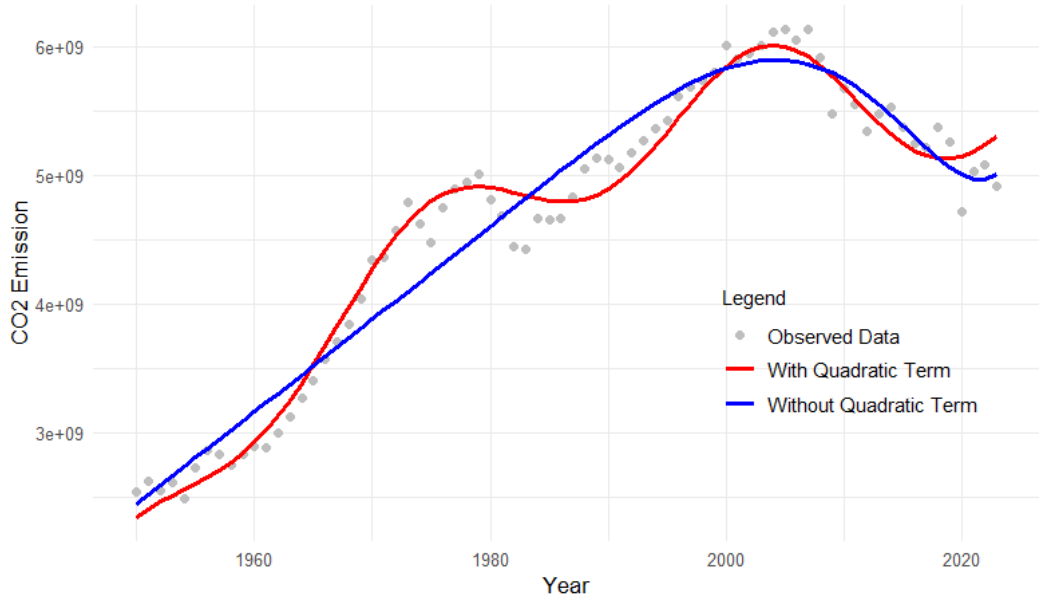

Figure 3. Fitting of the DE Solution to US CO_2 Emission Data, 1950–2023

Gray dots in Fig. 3 above represent observed data. The red line (with quadratic term) captures both trend and curvature, while the blue line (without quadratic term) illustrates a simpler trend fit.

The parameters c_1 and c_2, representing the initial oscillation amplitudes, also exhibit significant differences between the two models. In Model I, $c_1 = -2.992 \times 10^5$ and $c_2 = -2.992 \times 10^5$ are considerably smaller, indicating that this model fails to accurately represent the oscillation amplitudes. The low amplitude values in Model I suggest an overreliance on linear parameters to capture the global trend, thereby compromising the model's ability to describe oscillatory fluctuations. Conversely, Model II yields $c_1 = 1.790 \times 10^8$ and $c_2 = -2.216 \times 10^8$, demonstrating its superior capability to capture oscillatory behavior, particularly in the early period (1950–1980), as observed in the data. This highlights Model II's improved representation of dynamic fluctuations compared to Model I.

The quadratic component $c_3 t^2$ in Model II has a value of $c_3 = -9.652 \times 10^5$, which is crucial for capturing the patterns of acceleration and deceleration in the global trend. The parameter c_3 enables Model II to represent the curved pattern that cannot be captured by the linear and oscillatory components alone. The absence of the quadratic component in Model I forces the model to rely on the linear parameter c_4 and oscillations to describe the trend, resulting in unstable estimates for the other parameters.

The parameter c_5, representing the baseline, has a value of $c_5 = 2.451 \times 10^9$ in Model I and $c_5 = 2.167 \times 10^9$ in Model II. These values are relatively consistent and indicate that both models are capable of accurately capturing the initial CO_2 emission levels. However, Model II provides a more flexible representation of the global change patterns. The R^2 value further highlights the superiority of Model II ($R^2 = 97.7\%$) in capturing the overall data pattern. Meanwhile, the Root Mean Squared Error (RMSE) shows that Model II achieves lower error (RMSE = 0.1659) compared to Model I (RMSE=0.2531), indicating a closer fit to the observed data in terms of raw deviations. Furthermore, the Akaike Information Criterion (AIC) also supports this finding, where Model II yields the lowest value ($AIC = -251.90$) relative to Model I ($AIC = -191.35$). The lower AIC value implies that Model I provides a better trade-off between model complexity and goodness-of-fit. A visualization of the fitting results for both models to the CO_2emission data is shown in Fig. 3.

Model II (red line) demonstrates good performance in capturing the overall data pattern. Model II can follow the acceleration in CO_2 emissions before 2007 and the deceleration, thereafter, as indicated by the curved shape in the data. In contrast, Model I (blue line) shows that the model does not capture the oscillatory pattern as effectively and instead focuses more on the global quadratic trend. Therefore, the best solution model for modeling CO_2 emissions is Model II, as given by Eq. (20).

$$\mathcal{I}(t) = 1.790 \times 10^8 \exp(0.0068t)\cos(0.1841t) - 2.216 \times 10^8 \exp(0.0068t)\sin(0.1841t) \\ -9.652 \times 10^5 t^2 + 1.158 \times 10^8 t + 2.167 \times 10^9. \quad (20)$$

Overall, these results indicate that the model is not only capable of accommodating the long-term dynamics of CO_2 emissions but also effectively represents periodic fluctuations with good accuracy. The high performance of the model makes this model a reliable tool for explaining the historical patterns of CO_2 emissions and predicting future trends.

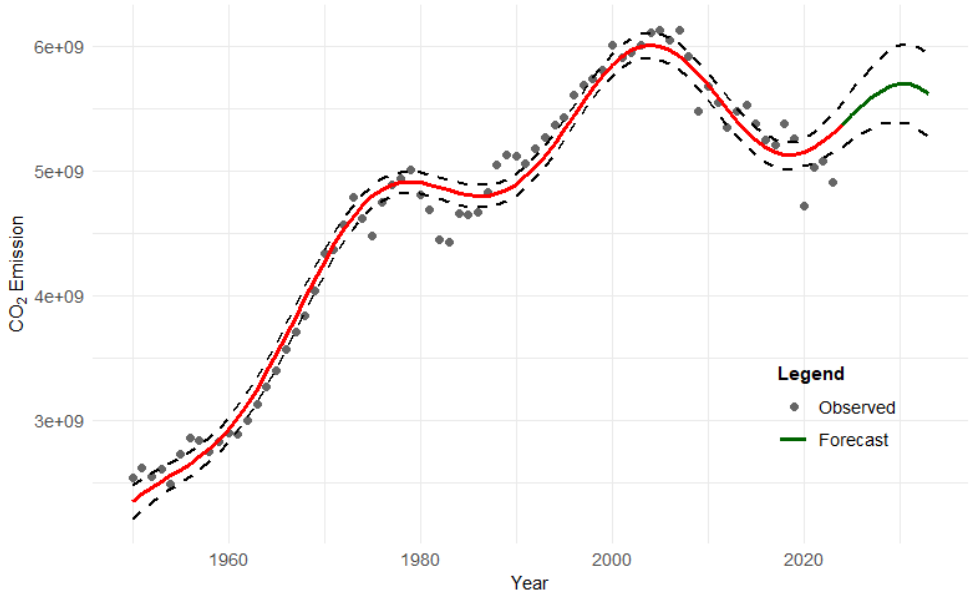

Figure 4. 10-year CO_2 Emission Prediction with 95% Bootstrap Confidence Interval

Gray dots represent observed historical data (1950–2023). The red line shows the fitted DE model, the dashed black lines represent the 95% bootstrap confidence interval, and the green line projects emissions for the forecast period (2024–2033). Fig. 4 shows the projected trajectory of CO_2 emission with 95% confidence interval in the US over 10 years ahead, based on Model II. The prediction intervals are estimated by using bootstrap resampling. This method aims to quantify the uncertainty of future predictions from the nonlinear model without making a specific assumption of error distribution. In this process, errors from the fitted model were resampled with replacement and added to the fitted values to generate a dataset. The model is trained on each bootstrap dataset to get new parameter estimates, which are then used to predict future emissions. This process is repeated 10,000 iterations, and quantiles are used to produce prediction intervals. The broadening interval band shows increasing uncertainty over time, as is common in extrapolative modeling. The prediction indicates a potential increase in CO_2 emissions occurring after 2023, following a relative decline in the early 2000s. This turning point and the model's oscillating behavior are compatible with the dynamic structure described by high-order DE.

This finding is particularly relevant when placed within the broader framework of US environmental policy, especially the decision to withdraw the US from the Paris climate agreement by President Donald Trump in early 2025 once again [31]. This withdrawal may impact the effectiveness of global climate mitigation efforts. Larch and Wanner [32] simulate that the US non-participation would eliminate more than a third of potential global emissions reduction (up to 31.8% through the reduction of national targets and 6.4% of the indirect impact of carbon leakage). Furthermore, Frumkin *et al.* [33] highlight that the implications of US withdrawal go beyond environmental degradation, posing a significant risk to public health and social resilience. From a geopolitical perspective, Macneil [34] argues that US participation in

global climate agreements has historically been a source of systemic instability due to domestic political events such as the recurrent cycle of withdrawal and re-engagement.

3.3 Economic Aspect of CO_2 Emissions

As discussed in the previous section, the US CO_2 emission data predicts a continued increase in emissions over the next decade. This projected trend, if one would realize, not only impacts the environmental and health concerns, but also entails considerable economic implications, especially in light of emerging international carbon pricing policies such as the European Union's Carbon Border Adjustment Mechanism (CBAM). From a financial perspective, these future economic costs must be evaluated through the lens of the time value of money [35], [36], recognizing that the monetary impact of delayed mitigation efforts may compound over time, making early action not only environmentally prudent but also economically advantageous.

The CBAM, formally legislated in 2023 and set for full implementation by 2026, imposes carbon tariffs on imports of carbon-intensive goods into the EU, aligning the carbon cost of imported goods with those produced under the EU Emissions Trading System (EU ETS). Sectors currently covered include steel, aluminum, cement, fertilizers, electricity, and hydrogen, industries in which the US is a significant exporter. Perdana and Vielle [37] emphasize that the absence of a domestic carbon pricing policy aligned with EU standards would result in greater CBAM prices for US exports in these industries. Their computable general equilibrium (CGE) modeling shows that unilateral CBAM implementation, particularly under increasing emission trajectories, reduces the competitiveness of non-EU exports that lack an equal carbon price.

The case in Vietnam further illustrates this point. Chu *et al.* [38] highlight how even a relatively small volume of impacted exports may lead to sectoral contraction and reduced export values due to CBAM application. Applied to the US, which exports billions of covered goods to the EU annually, the financial impact might be significantly greater, especially for small and medium-sized industries with little decarbonization capacity. Furthermore, a study by Zhu *et al.* [39] using GTAP-E simulations shows that the CBAM deteriorates the terms of trade of nations with growing emissions while improving those of the EU. This implies a macroeconomic disadvantage for the US if emissions continue to increase and carbon-pricing policies are not implemented domestically.

From a trade policy perspective, the growing divergence between U.S. emission trends and EU climate ambitions may trigger adverse trade effects beyond direct CBAM costs. Dobranschi *et al.* [40] argue that countries with slower adoption of low-carbon technologies may face output relocation and even retaliatory trade measures. To mitigate these risks, Elder *et al.* [41] suggest adopting domestic carbon-pricing or equivalent mitigation policies, accelerating industrial decarbonization and carbon valuation strategies, and engaging in climate clubs or bilateral alignment mechanisms with the EU.

Thus, the projected increase in US emissions not only indicates an environmental trend but also implies an economic burden, directly through CBAM tariffs and indirectly through trade diversion, sectoral devaluation, and loss of geopolitical economic influence. It is important to note that while the model accurately captures historical emission patterns, it does not include explicit covariates related to policy decisions, energy transitions, or economic shocks. Therefore, any interpretation of the forecast considering political events should be made with caution. While such events may plausibly affect future emissions, this relationship is not directly modeled in the differential framework used here.

3.4 Future Research

To enhance the robustness of the proposed high-order differential equation model, future research will extend the framework by incorporating spatial dimensions that reflect the interconnected nature of regional emission dynamics. Specifically, the Generalized Space-Time Autoregressive (GSTAR) model [42], [43] will be integrated to capture both spatial dependencies and temporal dynamics across regions. This approach allows the modeling of emission interdependencies between neighboring states or regions, acknowledging that environmental and economic activities in one location can influence others. By introducing spatial autoregressive terms, the GSTAR model can account for regional emission and improve predictive accuracy in a geographically disaggregated setting. This enhancement is particularly relevant for evaluating localized policy impacts and identifying regional emission hotspots under various regulatory scenarios.

In addition to spatial considerations, multivariate categorical analysis will be incorporated using the Burt matrix [44], which effectively handles complex interactions among discrete socio-economic and policy

variables. Variables such as energy portfolio composition, industrial activity types, and regulatory stringency levels will be encoded into this matrix structure to explore their joint influence on emission trends. The Burt matrix serves as a foundation for applying techniques like Multiple Correspondence Analysis (MCA), which can reveal latent associations and clusters within the categorical data. Integrating this analysis into the overall modeling framework will enable researchers to systematically identify structural factors that contribute to regional differences in emission behaviors and support policy differentiation based on socio-economic contexts.

Finally, to address uncertainty and quantify the risks associated with future emission trajectories, probability-based modeling will be incorporated into the analytical framework. Such models provide an approach to characterize the likelihood of various emission outcomes under different policies, technological, or economic scenarios. By embedding stochastic components into the differential and spatio-temporal structures, this extension allows for the estimation of failure probabilities [45], including the risk of exceeding carbon targets or policy thresholds, and enhances the capacity of the model to support robust, risk-informed decision-making. This probabilistic aspect introduces a critical dimension of realism, enabling more comprehensive assessments of environmental and regulatory outcomes in the face of uncertainty.

4. CONCLUSION

This study successfully developed a high-order differential equation model capable of capturing three key features in the dynamics of CO_2 emissions in the US: (1) a long-term linear trend, (2) a quadratic component indicating acceleration or deceleration in the rate of emission growth, and (3) oscillatory behavior reflecting short-term periodic fluctuations. By integrating nonlinear estimation techniques into the model formulation, the parameters were empirically fitted to historical emission data with a high degree of accuracy and statistical significance. The fitting results show that the proposed model not only accurately fits historical emission trajectories but also offers strong predictive capacity for future emission dynamics. The model's projections suggest a continued increase in emissions over the next decade, with important implications for environmental policy, especially regarding international mechanisms such as the European Union's Carbon Border Adjustment Mechanism (CBAM). Methodologically, this study highlights the effectiveness of combining high-order differential equation structures with nonlinear parameter estimation to model the complex temporal behavior of carbon emissions. As a flexible and extensible modeling framework, it can be further enhanced by incorporating exogenous drivers through integration with established analytical models such as STIRPAT. Such integration would support more comprehensive scenario analyses and inform policy design aimed at mitigating carbon emissions in both domestic and global contexts.

Author Contributions

Udjianna S. Pasaribu: Conceptualization, methodology, Formal Analysis, Writing-Original Draft, Writing-Review and Editing, Funding Acquisition. Adilan W. Mahdiyasa: Conceptualization, Data Curation, Formal Analysis, Writing-Original Draft, Writing-Review and Editing. Asrul Irfanullah: Formal Analysis, Methodology, Validation, Software, Writing-Original Draft, Writing-Review and Editing. All authors discussed the results and contributed to the final manuscript.

Funding Statement

This work was funded by ITB Research Programme 2025 "Riset Unggulan ITB" with grant number 841/IT1.B07.1/TA.00/2025

Acknowledgment

We would like to thank four anonymous reviewers for their insightful and constructive comments.

Declarations

The authors declare no competing interests.

Declaration of Generative AI and AI-assisted Technologies

Generative AI tools (e.g., ChatGPT) were used solely for language refinement, including grammar, spelling, and clarity. The scientific content, analysis, interpretation, and conclusions were developed entirely by the authors. All final text was reviewed and approved by the authors.

REFERENCES

[1] WMO, "STATE OF THE GLOBAL CLIMATE 2023," *World Meteorological Organization*, 2024.

[2] D. K. Espoir and R. Sunge, "CO2 EMISSIONS AND ECONOMIC DEVELOPMENT IN AFRICA: EVIDENCE FROM A DYNAMIC SPATIAL PANEL MODEL," *Journal of Environmental Management*, vol. 300, p. 113617, 2021. doi: https://doi.org/0.1016/j.jenvman.2021.113617.

[3] A. W. Mahdiyasa, D. J. Large, B. P. Muljadi, M. Icardi, and S. Triantafyllou, "MPEAT—A FULLY COUPLED MECHANICAL-ECOHYDROLOGICAL MODEL OF PEATLAND DEVELOPMENT," *Ecohydrology*, vol. 15, no. 1, p. e2361, 2022. doi: https://doi.org/10.1002/eco.2361.

[4] A. W. Mahdiyasa, D. J. Large, M. Icardi, and B. P. Muljadi, "MPEAT2D – A FULLY COUPLED MECHANICAL–ECOHYDROLOGICAL MODEL OF PEATLAND DEVELOPMENT IN TWO DIMENSIONS," *Earth Surface Dynamics*, vol. 12, no. 4, pp. 929–952, 2024. doi: https://doi.org/10.5194/esurf-12-929-2024.

[5] F. Ren and D. H. Long, "CARBON EMISSION FORECASTING AND SCENARIO ANALYSIS IN GUANGDONG PROVINCE BASED ON OPTIMIZED FAST LEARNING NETWORK," *J Cleaner Production*, vol. 317(6), 2021. doi: https://doi.org/10.1016/j.jclepro.2021.128408.

[6] A. W. Mahdiyasa, D. J. Large, B. P. Muljadi, and M. Icardi, "MODELLING THE INFLUENCE OF MECHANICAL-ECOHYDROLOGICAL FEEDBACK ON THE NONLINEAR DYNAMICS OF PEATLANDS," *Ecological Modelling*, vol. 478, p. 110299, 2023. doi: https://doi.org/10.1016/j.ecolmodel.2023.110299.

[7] U. Mukhaiyar *et al.*, "THE GENERALIZED STAR MODELLING WITH THREE-DIMENSIONAL OF SPATIAL WEIGHT MATRIX IN PREDICTING THE INDONESIA PEATLAND'S WATER LEVEL," *Environmental Sciences Europe*, vol. 36, no. 1, p. 180, 2024. doi: https://doi.org/10.1186/s12302-024-00979-6.

[8] M. Gao, H. Yang, Q. Goh, "A NOVEL METHOD FOR CARBON EMISSION FORECASTING BASED ON GOMPERTZ'S LAW AND FRACTIONAL GREY MODEL: EVIDENCE FROM AMERICAN INDUSTRIAL SECTOR," *Renewable Energy*, vol. 181, pp. 803–819, Jan. 2022. doi: https://doi.org/10.1016/j.renene.2021.09.072.

[9] A. P. Ozora Situngkir, A. W. Mahdiyasa, K. N. Sari, and U. S. Pasaribu, "MODELLING PEATLAND FIRE RISK AND ECONOMIC LOSSES IN INDONESIA," in *2025 5th International Conference on Innovative Research in Applied Science, Engineering and Technology (IRASET)*, May 2025, pp. 1–6. doi: https://doi.org/10.1109/IRASET64571.2025.11008022.

[10] A. W. Mahdiyasa, U. S. Pasaribu, and B. P. Muljadi, "MECHANICAL STABILITY MODELLING OF PEATLAND WITH COUPLED HYDRO-MECHANICAL APPROACH," in *2025 5th International Conference on Innovative Research in Applied Science, Engineering and Technology (IRASET)*, May 2025, pp. 1–7. doi: https://doi.org/10.1109/IRASET64571.2025.11008015.

[11] K. N. Sari, U. S. Pasaribu, U. Mukhaiyar, A. W. Mahdiyasa, D. N. Choesin, and F. Al'Muzakki, "PREDICTION OF GROUNDWATER LEVELS TO MITIGATE THE RISK OF INCREASED CARBON EMISSIONS DUE TO PEATLAND FIRES THROUGH ANISOTROPIC SEMIVARIOGRAM MODELING WITH OUTLIER MODIFICATION," in *Proceedings of International Conference on Computers and Industrial Engineering, (CIE)*, 2024, pp. 1761–1774.

[12] EEA, "ATMOSPHERIC GREENHOUSE GAS CONCENTRATION," *European Environment Agency*, 2024. https://www.eea.europa.eu/en/analysis/indicators/atmospheric-greenhouse-gas-concentrations?activeAccordion=ecdb3bcf-bbe9-4978-b5cf-0b136399d9f8 (accessed Aug. 13, 2024).

[13] R. C. Kafle, K. P. Pokhrel, N. Khanal, and C. P. Tsokos, "DIFFERENTIAL EQUATION MODEL OF CARBON DIOXIDE EMISSION USING FUNCTIONAL LINEAR REGRESSION," *Journal of Applied Statistics*, vol. 46, no. 7, pp. 1246–1259, 2019. doi: https://doi.org/10.1080/02664763.2018.1542667.

[14] AON, "CLIMATE AND CATASTROPHE INSIGHT," 2024. [Online]. Available: https://assets.aon.com/-/media/files/aon/reports/2024/climate-and-catastrophe-insights-report.pdf

[15] NCEI, "U.S. BILLION-DOLLAR WEATHER AND CLIMATE DISASTERS," *NOAA National Centers for Environmental Information*, 2024. https://www.ncei.noaa.gov/access/billions / (accessed Jan. 09, 2024).

[16] Z. Wei, K. Wei, and J. Liu, "DECOUPLING RELATIONSHIP BETWEEN CARBON EMISSIONS AND ECONOMIC DEVELOPMENT AND PREDICTION OF CARBON EMISSIONS IN HENAN PROVINCE: BASED ON TAPIO METHOD AND STIRPAT MODEL," *Environmental Science and Pollution Research*, vol. 30, no. 18, pp. 52679–52691, 2023. doi: https://doi.org/10.1007/s11356-023-26051-z.

[17] S. Wang, T. Zhao, H. Zheng, and J. Hu, "THE STIRPAT ANALYSIS ON CARBON EMISSION IN CHINESE CITIES: AN ASYMMETRIC LAPLACE DISTRIBUTION MIXTURE MODEL," *Sustainability (Switzerland)*, vol. 9, no. 12, 2017. doi: https://doi.org/10.3390/su9122237.

[18] E. M. Farouki and S. Aissaoui, "NEXUS BETWEEN ECONOMY, RENEWABLE ENERGY, POPULATION AND ECOLOGICAL FOOTPRINT: EMPIRICAL EVIDENCE USING STIRPAT MODEL IN MOROCCO," *Procedia Computer Science*, vol. 236, pp. 67–74, 2024. doi: https://doi.org/10.1016/j.procs.2024.05.005.

[19] D. C. Pattak *et al.*, "THE DRIVING FACTORS OF ITALY'S CO2 EMISSIONS BASED ON THE STIRPAT MODEL: ARDL, FMOLS, DOLS, AND CCR APPROACHES," *Energies*, vol. 16, no. 15, pp. 1–21, 2023. doi: https://doi.org/10.3390/en16155845.

[20] J. M. Montero, G. Fernández-Avilés, and T. Laureti, "A LOCAL SPATIAL STIRPAT MODEL FOR OUTDOOR NOX CONCENTRATIONS IN THE COMMUNITY OF MADRID, SPAIN," *Mathematics*, vol. 9, no. 6, 2021. doi: https://doi.org/10.3390/math9060677.

[21] C. Rao, Q. Huang, L. Chen, M. Goh, and Z. Hu, "FORECASTING THE CARBON EMISSIONS IN HUBEI PROVINCE

UNDER THE BACKGROUND OF CARBON NEUTRALITY: A NOVEL STIRPAT EXTENDED MODEL WITH RIDGE REGRESSION AND SCENARIO ANALYSIS," *Environmental Science and Pollution Research*, vol. 30, no. 20, pp. 57460–57480, 2023. doi: https://doi.org/10.1007/s11356-023-26599-w.

[22] T. J. Goreau, "BALANCING ATMOSPHERIC CARBON DIOXIDE," *AMBIO*, vol. 19, pp. 230–236, 1990, [Online]. Available: https://www.jstor.org/stable/4313702

[23] C. P. Tsokos and Y. Xu, "MODELING CARBON DIOXIDE EMISSIONS WITH A SYSTEM OF DIFFERENTIAL EQUATIONS," *Nonlinear Analysis, Theory, Methods and Applications*, vol. 71, no. 12, pp. e1182–e1197, 2009. doi: https://doi.org/10.1016/j.na.2009.01.146.

[24] L. Han, H. Sui, and Y. Ding, "MATHEMATICAL MODELING AND STABILITY ANALYSIS OF A DELAYED CARBON ABSORPTION-EMISSION MODEL ASSOCIATED WITH CHINA'S ADJUSTMENT OF INDUSTRIAL STRUCTURE," *Mathematics*, vol. 10, no. 17, 2022. doi: https://doi.org/10.3390/math10173089.

[25] P. Donald, M. Mayengo, and A. G. Lambura, "MATHEMATICAL MODELING OF VEHICLE CARBON DIOXIDE EMISSIONS," *Heliyon*, vol. 10, no. 2, p. e23976, 2024. doi: https://doi.org/10.1016/j.heliyon.2024.e23976.

[26] I. Mukhartova, J. Kurbatova, D. Tarasov, R. Gibadullin, A. Sogachev, and A. Olchev, "MODELING TOOL FOR ESTIMATING CARBON DIOXIDE FLUXES OVER A NON-UNIFORM BOREAL PEATLAND," *Atmosphere*, vol. 14, no. 4, pp. 1–21, 2023. doi: https://doi.org/10.3390/atmos14040625.

[27] R. Haberman, *MATHEMATICAL MODEL: MECHANICAL VIBRATIONS, POPULATION DYNAMICS, AND TRAFFIC FLOW. AN INTRODUCTION TO APPLIED MATHEMATICS*. New Jersey: SIAM, 1998. doi: https://doi.org/10.1137/1.9781611971156

[28] G. A. F. Seber and C. J. Wild, *NONLINEAR REGRESSION*. Canada: Wiley-Interscience, 2003.doi: https://doi.org/10.1002/9780471722199

[29] A. Bjorck, *NUMERICAL METHOD FOR LEAST SQUARES PROBLEM*. Siam, 1996. doi: https://doi.org/10.1137/1.9781611971484.

[30] P. Team, "RSTUDIO: INTEGRATED DEVELOPMENT ENVIRONMENT FOR R." Posit Software, PBC, Boston, 2025. [Online]. Available: http://www.posit.co/

[31] E. Lazarou and G. Leclerc, "US WITHDRAWAL FROM THE PARIS CLIMATE AGREEMENT AND FROM THE WHO," 2025.

[32] M. Larch and J. Wanner, "THE CONSEQUENCES OF NON-PARTICIPATION IN THE PARIS AGREEMENT," *European Economic Review*, vol. 163, 2024. doi: https://doi.org/10.1016/j.euroecorev.2024.104699.

[33] H. Frumkin, A. Haines, and M. Rao, "THE USWITHDRAWAL FROM THE PARIS CLIMATE AGREEMENT: COULD IT TRUMP PROGRESS ON CLIMATE CHANGE AND HEALTH?," London, 2025. doi: https://doi.org/10.1136/bmj.r185.

[34] R. MacNeil, "THE CASE FOR A PERMANENT US WITHDRAWAL FROM THE PARIS ACCORD," *AUSTRALIAN JOURNAL OF INTERNATIONAL AFFAIRS*, 2025. doi: https://doi.org/10.1080/10357718.2025.2482701.

[35] A. Widyawan, U. S. Pasaribu, Henintyas, and D. Permana, "ESTIMATION OF CUSTOMER LIFETIME VALUE OF A HEALTH INSURANCE WITH INTEREST RATES OBEYING UNIFORM DISTRIBUTION," 2015. doi: https://doi.org/10.1063/1.4936458

[36] A. W. Mahdiyasa, U. S. Pasaribu, and K. N. Sari, "MODELING CUSTOMER LIFETIME VALUE WITH MARKOV CHAIN IN THE INSURANCE INDUSTRY," *Barekeng*, vol. 19, no. 1, 2025. doi: https://doi.org/10.30598/barekengvol19iss1pp687-696.

[37] S. Perdana and M. Vielle, *CARBON BORDER ADJUSTMENT MECHANISM IN THE TRANSITION TO NET-ZERO EMISSIONS: COLLECTIVE IMPLEMENTATION AND DISTRIBUTIONAL IMPACTS*, vol. 25. Springer Japan, 2023. doi: https://doi.org/10.1007/s10018-023-00361-5.

[38] H. L. Chu *et al.*, "THE ECONOMIC IMPACTS OF THE EUROPEAN UNION'S CARBON BORDER ADJUSTMENT MECHANISM ON DEVELOPING COUNTRIES: THE CASE OF VIETNAM," *Fulbright Review of Economics and Policy*, vol. 4, no. 1, pp. 1–17, 2024. doi: https://doi.org/10.1108/FREP-03-2024-0011.

[39] J. Zhu, Y. Zhao, and L. Zheng, "THE IMPACT OF THE EU CARBON BORDER ADJUSTMENT MECHANISM ON CHINA'S EXPORTS TO THE EU," *Energies*, vol. 17, no. 2, 2024. doi: https://doi.org/10.3390/en17020509.

[40] M. Dobranschi, D. Nerudová, V. Solilová, and K. Stadler, "CARBON BORDER ADJUSTMENT MECHANISM CHALLENGES AND IMPLICATIONS: THE CASE OF VISEGRÁD COUNTRIES," *Heliyon*, vol. 10, 2024. doi: https://doi.org/10.1016/j.heliyon.2024.e30976.

[41] M. Elder, S. Hopkinson, X. Zhou, Y. Arino, and K. Matsushita, "IMPLICATIONS OF THE EU'S CARBON BORDER ADJUSTMENT MECHANISM (CBAM) FOR ASEAN: AN ARGUMENT FOR MORE AMBITIOUS CARBON PRICING," 2025.

[42] U. Mukhaiyar, A. W. Mahdiyasa, T. Prastoro, B. C. Suherlan, U. S. Pasaribu, and S. W. Indratno, "SPATIAL AND TIME SERIES MODELLING FOR THE GROUNDWATER LEVEL OF PEATLANDS IN RIAU AND CENTRAL KALIMANTAN, INDONESIA," in *Decision Mathematics, Statistical Learning and Data Mining*, W. F. Wan Yaacob, Y. B. Wah, and O. U. Mehmood, Eds. Springer Nature Singapore, 2024, pp. 89–104. doi: https://doi.org/10.1007/978-981-97-3450-4_7

[43] U. Mukhaiyar, A. W. Mahdiyasa, K. N. Sari, and N. T. Noviana, "THE GENERALIZED STAR MODELING WITH MINIMUM SPANNING TREE APPROACH OF SPATIAL WEIGHT MATRIX," *Frontiers in Applied Mathematics and Statistics*, vol. 10, 2024. doi: https://doi.org/10.3389/fams.2024.1417037

[44] A. W. Mahdiyasa and U. S. Pasaribu, "MULTIPLE CORRESPONDENCE ANALYSIS USING BURT MATRIX: A STUDY OF BANDUNG INSTITUTE OF TECHNOLOGY STUDENT CHARACTERISTICS," in *IOP Conference Series: Materials Science and Engineering*, 2019, vol. 598, no. 1, p. 12012. doi: https://doi.org/10.1088/1757-899X/598/1/012012.

[45] A. W. Mahdiyasa and A. Grahito, "PROBABILITY OF FAILURE MODEL IN MECHANICAL COMPONENT BECAUSE OF FATIGUE," in *Journal of Physics: Conference Series*, 2019, vol. 1245, no. 1, p. 12053. doi: https://doi.org/10.1088/1742-6596/1245/1/012053